JACS
JOURNAL OF THE AMERICAN CHEMICAL SOCIETY
Communication
pubs.acs.org/JACS

In Situ Confinement of Ultrasmall Pd Clusters within Nanosized Silicalite-1 Zeolite for Highly Efficient Catalysis of Hydrogen Generation

Ning Wang,[†,‡] Qiming Sun,[†,‡] Risheng Bai,[†] Xu Li,[†] Guanqi Guo,[†] and Jihong Yu*[,†]

[†]State Key Laboratory of Inorganic Synthesis and Preparative Chemistry, College of Chemistry, Jilin University, Changchun 130012, P.R. China

Supporting Information

ABSTRACT: Well-dispersed and ultrasmall Pd clusters in nanosized silicalite-1 (**MFI**) zeolite have been prepared under direct hydrothermal conditions using $[Pd(NH_2CH_2CH_2NH_2)_2]Cl_2$ as precursor. High-resolution scanning transmission electron microscopy studies indicate that the Pd clusters are encapsulated within the intersectional channels of **MFI**, and the Pd clusters in adjacent channels visually aggregate, forming nanoparticles (NPs) of ∼1.8 nm. The resultant catalysts show an excellent activity and highly efficient H_2 generation toward the complete decomposition of formic acid (FA) under mild conditions. Notably, thanks to the further reduced Pd NP size (∼1.5 nm) and the additionally introduced basic sites, the Pd/S-1-in-K catalyst affords turnover frequency values up to 856 h^{-1} at 25 °C and 3027 h^{-1} at 50 °C. The easy in situ confinement synthesis of metal clusters in zeolites endows the catalysts with superior catalytic activities, excellent recyclability, and high thermal stability, thus opening new perspectives for the practical application of FA as a viable and effective H_2 storage material for use in fuel cells.

Hydrogen is considered to be an environmentally attractive fuel and a promising efficient energy carrier for future applications because of its high energy density and renewability.[1] However, safe and efficient storage and release of H_2 remains a bottleneck and a challenge for a fuel-cell-based hydrogen economy.[2] Recently, formic acid (FA), a product of biomass possessing a high H_2 content (4.4 wt%) and outstanding stability, that is nontoxic and easily recharged, has proven to be a safe and suitable hydrogen carrier for portable H_2 storage applications.[3] Hydrogen stored in FA can be released via a dehydrogenation pathway ($HCOOH \rightarrow H_2+CO_2$) over suitable catalysts. But, from the perspective of H_2 storage applications, the undesirable dehydration reaction ($HCOOH \rightarrow H_2O+CO$) should be avoided because CO easily leads to catalyst poisoning in fuel cells.[4]

In recent years, many homogeneous catalysts have been intensively investigated, showing excellent performance for FA dehydrogenation.[5] Yet, several drawbacks, such as fast deactivation, difficulty to separate and recycle, and use of organic solvents, hinder their further utility. To overcome these shortcomings, heterogeneous catalysts have attracted tremendous and increasing interest.[3c,6] Several types of support materials for metal nanoparticles (NPs) have been employed in FA decomposition reactions, including graphene oxide,[7] nanoporous carbon,[3d] and metal−organic frameworks.[4a,8] However, some of these catalysts suffer from relatively poor recyclability and lower thermal stability. Hence, developing highly efficient and stable catalysts for FA decomposition also remains a challenge.

Zeolites have drawn growing attention as ideal supports for confinement synthesis of metal NPs due to their well-defined channels, tunable acidity and basicity, and high thermal and chemical stability.[9] The zeolite matrix could restrain aggregation of the metal NPs, thus enhancing the catalytic activity and recycling stability of the catalysts. In general, the NPs were supported on zeolites by ion exchange[10] and wetness impregnation.[11] However, these methods may lead to large and nonuniform NPs as well as poor dispersion and unsatisfactory catalytic activity.[12] Recently, Iglesia et al. developed a synthetic protocol for encapsulating series of smaller metal clusters within different types of aluminosilicate zeolites, such as **BEA**, **FAU**, **SOD**, **LTA**, etc., by a ligand-stabilized method and **MFI** via inter-zeolite transformation.[13] Notably, silicalite-1 with **MFI** zeotype is an ideal catalyst support for a number of industrial processes, but until now, in situ encapsulation of ultrasmall metal clusters within **MFI** structure under direct hydrothermal conditions has been unsuccessful.

Herein, ultrasmall Pd clusters encapsulated within nanosized silicalite-1 (S-1) zeolite have been, for the first time, successfully synthesized under direct hydrothermal conditions using $[Pd(NH_2CH_2CH_2NH_2)_2]Cl_2$ as precursor and tetrapropylammonium hydroxide (TPAOH) as template. The resultant catalysts exhibit superior activity and efficient H_2 generation, without forming CO, toward the complete decomposition of FA. Strikingly, when KOH was introduced into the synthesis gel, the Pd/S-1-in-K catalyst with basic sites and further reduced size of metal clusters showed enhanced catalytic activity, affording excellent turnover frequency (TOF) values as high as 856 h^{-1} at 25 °C and 3027 h^{-1} at 50 °C, reflecting some of the highest activity for heterogeneously catalyzed FA decomposition under similar conditions.

Ultrasmall Pd clusters in situ encapsulated within nanosized S-1 zeolite (Pd/S-1-in) were synthesized in a starting gel with the molar composition of 1.0 SiO_2:0.4 TPAOH:35 H_2O:0.0045 $[Pd(NH_2CH_2CH_2NH_2)_2]Cl_2$ under hydrothermal conditions at 170 °C for 4 days, followed by H_2 reduction. Raman

Received: April 5, 2016
Published: June 1, 2016

DOI: 10.1021/jacs.6b03518
J. Am. Chem. Soc. 2016, 138, 7484−7487

Scheme 1. Confinement Synthesis of Pd Clusters within Nanosized Silicalite-1 Zeolite

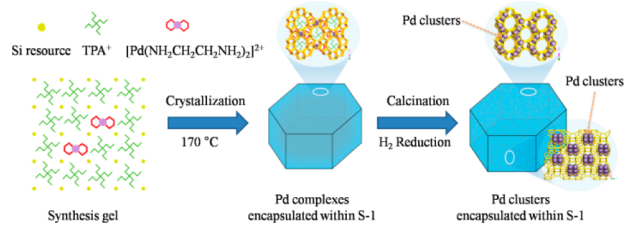

spectroscopy, thermogravimetry−differential thermal analysis, and ^{13}C MAS NMR analyses confirm that the $[Pd(NH_2CH_2CH_2NH_2)_2]Cl_2$ complex stays intact inside the as-synthesized zeolite (Figures S1−S3). To generate basicity in the Pd/S-1-in catalysts that may benefit the cleavage of the O−H bonds in FA molecules and further improve the activity of FA decomposition,[7a] NaOH and KOH were introduced into the synthesis gel to prepare Pd/S-1-in-Na and Pd/S-1-in-K, respectively, under conditions similar to those used for Pd/S-1-in. The process for the synthesis of Pd/S-1-in catalyst is illustrated in Scheme 1. First, the Pd complexes interact with the initial zeolitic gel and are encapsulated into the zeolite framework by self-assembly during crystallization process. Upon calcination in air and reduction by H_2, the ultrasmall Pd clusters can be finally confined inside the nanosized S-1 zeolite. The specific sites of Pd clusters within the S-1 zeolite will be discussed in a later section. For comparison, the Pd/S-1-im catalyst was also synthesized by impregnation using the incipient wetness method with $(NH_4)_2PdCl_4$ solution, and the Pd/C catalyst was obtained from a commercial Pd/C catalyst following H_2 reduction treatment at 200 °C for 2 h.

As shown in Figure S4, the X-ray diffraction patterns of all of the Pd cluster-containing zeolite catalysts show peaks characteristic of the **MFI** structure, without detectable peaks corresponding to Pd or oxide crystal structures, indicating the absence of large Pd species in the as-synthesized samples.

Transmission electron microscopy (TEM) images and scanning transmission electron microscopy (STEM) images, as well as the size distributions of Pd clusters in the synthesized samples after calcination and H_2 reduction, are shown in Figures S5 and 1, respectively. TEM images show that the Pd clusters encapsulated within nanosized S-1 zeolites are well dispersed and uniformly distributed throughout the zeolite crystals. The average sizes of Pd clusters in situ encapsulated within the nanosized S-1 zeolite are in the range of 1.5−1.8 nm, which are much smaller than those of impregnation-prepared Pd/S-1-im catalyst (2.7 nm) and the commercial Pd/C catalyst (3.8 nm). Notably, the introduction of alkali hydroxide in the synthesis gel could further decrease the Pd clusters size because the alkali cations may reduce some void spaces of the channels.

The visually observed sizes of Pd NPs appear much larger than those of the **MFI** channels (0.53 × 0.56 nm) as well as intersectional channels (~0.9 nm).[14] High-resolution STEM was used to investigate the location of Pd clusters inside the crystals of Pd/S-1-in-K. The intact and empty straight channels can clearly be observed (Figure 2a), suggesting that most of the Pd clusters might be located in the intersectional void spaces between the straight and sinusoidal channels of the **MFI** structure. When the view is changed to another orientation, the Pd clusters appear as rod-like aggregates (Figure 2b). Corresponding schematic crystallographic projections of Pd

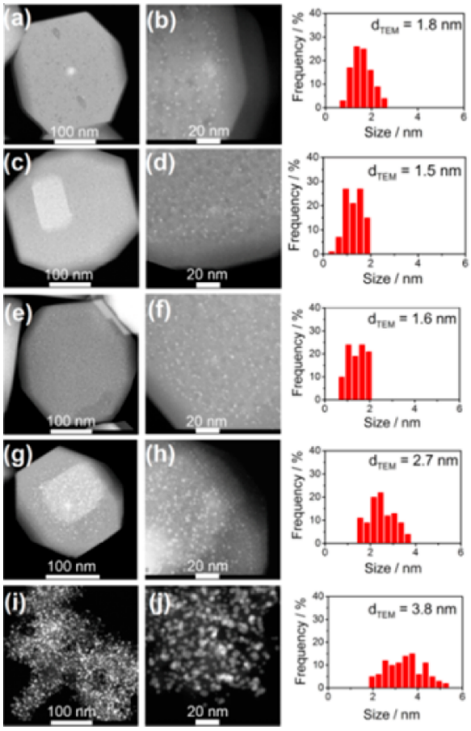

Figure 1. STEM images of Pd/S-1-in (a,b), Pd/S-1-in-K (c,d), Pd/S-1-in-Na (e,f), Pd/S-1-im (g,h), and Pd/C (i,j) samples and corresponding size distributions of Pd clusters. Surface-weighted mean cluster diameter $d_{TEM} = \sum n_i d_i^3 / \sum n_i d_i^2$, where n_i is the number of crystallites having diameter d_i.

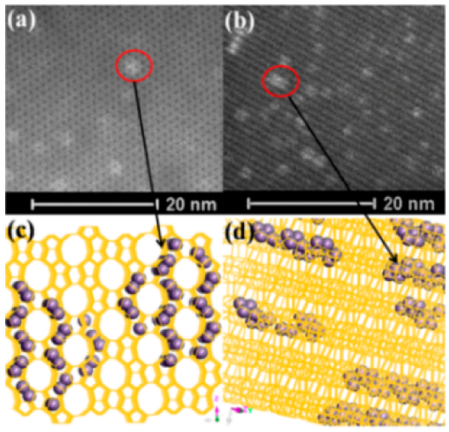

Figure 2. High-resolution STEM images (a,b) of Pd/S-1-K sample and corresponding schematic crystallographic projections (c,d) of **MFI** viewed from different orientations.

clusters inside the intersectional channels in S-1 are shown in Figure 2c,d. Strikingly, the ultrasmall Pd clusters (0.3−0.6 nm) in the Pd/S-1-in-K catalyst can be observed (Figure S6). The large size of Pd NPs observed in Figure 1 might be due to the visual aggregation of Pd clusters within the adjacent channels. In addition, all of the calcined zeolitic samples show almost identical ^{29}Si MAS NMR spectra (Figure S7), which further demonstrates that the encapsulated Pd clusters do not break the zeolite framework and the zeolite framework remains intact.

Simulated annealing calculations were also performed using universal force field to study the location of the guest species in the channels. Figure S8 presents the optimal structure model with the lowest energy. The results show that the tetrapropyl-

DOI: 10.1021/jacs.6b03518
J. Am. Chem. Soc. 2016, 138, 7484−7487

ammonium cations (TPA^+) locate in the center of the straight 10-ring channels along the *b* direction and the $[Pd(NH_2CH_2CH_2NH_2)_2]^{2+}$ cations in the intersectional channels. Some hydroxyl anions also exist in the crystal structure to balance the positive charges. After the TPA^+ and ethylenediamine ligands were removed, the simulation results indicated that the ultrasmall Pd clusters are preferably located in the intersectional void spaces between the straight and sinusoidal channels, which is in accordance with the observed STEM images.

To further verify that the Pd clusters are encapsulated within the zeolite crystals rather than on the crystal surface, shape-selective reductions of nitrobenzene and 3-nitrotoluene were performed over the Pd/S-1-in catalyst and the Pd/C catalyst. According to the UV/vis spectra and gas chromatography−mass spectrometry (GC-MS) analyses (Figures S9−S13), the Pd/C catalyst exhibited 100% conversion for the reduction of both nitrobenzene and 3-nitrotoluene. In contrast, the Pd/S-1-in catalyst showed 100% conversion only for the reduction of nitrobenzene, but no activity for the reduction of 3-nitrotoluene, which cannot enter into the zeolite channels due to its bulky molecular size. These results further prove that the Pd clusters are encapsulated inside the zeolite crystals instead of located on the crystal surface.

The STEM image of Pd/S-1-in-K, corresponding high-angle annular dark-field STEM images, and elemental mappings for Si, Pd, and K are shown in Figure S14. It can be seen that Pd and K are uniformly distributed throughout the S-1 zeolite crystals. The energy-dispersive X-ray (EDX) spectrum further confirms the existence of Pd and K in the sample. All of the Pd cluster-containing zeolites possess similar metal loadings of ~0.63−0.65 wt%, as measured by inductively coupled plasma atomic emission spectroscopy (ICP-AES) analysis (Table S1), and the amounts of Na and K are 0.21 and 0.62 wt% in samples Pd/S-1-in-Na and Pd/S-1-in-K, respectively. N_2 adsorption measurements show that some decrease in micropore area of ~20 m^2/g can be observed for the Pd/S-1 sample as compared to the S-1 zeolite, indicating that the dispersed Pd clusters are occupied inside the pores of S-1 zeolites. However, the Pd/S-1-in sample still possesses sufficient void space (191 m^2/g) for the reactant transfer (Figure S15). Temperature-programmed desorption spectra of CO_2 reveal that the Pd/S-1-in-Na and Pd/S-1-in-K samples possess some basicity due to the introduction of alkali cations onto the zeolite (Figure S16).[15] Moreover, the Pd clusters' dispersion values, estimated from H_2 chemisorption of sample Pd/S-1-K, are the highest compared to other samples, indicating that more metal cluster surfaces are available for catalytic reaction (Table S1).

X-ray photoelectron spectroscopy (XPS) of the Pd/C sample (Figure S14c) shows two peaks at 335.7 and 341.0 eV, attributed to the $Pd3d_{5/2}$ and $Pd3d_{3/2}$ of Pd(0), respectively.[3d] However, no XPS signals were observed in the Pd/S-1-in-K sample because the Pd clusters were confined inside the zeolites. When the Pd/S-1-in-K sample was dissolved in NaOH solution, peaks at 335.1 and 340.4 eV could be observed that correspond to the typical Pd metal with valence of zero.[16]

Significantly, the sample Pd/S-1-in exhibited remarkably improved thermal stability compared to Pd/C and Pd/S-1-im. As shown in Figure S17, after calcination at 700 °C for 2 h under N_2 atmosphere, the Pd particles in Pd/C were almost entirely sintered, and the diameter of Pd particles increased from ~3.8 to ~27 nm. In contrast, the Pd/S-1-in sample showed less change in Pd particles' size, from ~1.8 to ~2.3 nm. Moreover, the Pd/S-1-in sample also exhibited good stability in H_2 and O_2 atmosphere

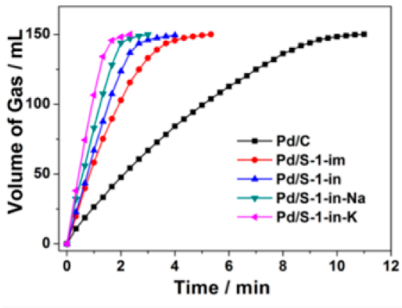

Figure 3. Volume of the generated gas (CO_2 + H_2) versus time for the dehydrogenation of FA-SF (1:1) solution over Pd/C and Pd/S-1 catalysts at 50 °C (n_{Pd}/n_{FA} = 0.01).

as well as during aging treatments at 600 °C in the presence of water (Figures S18−S20). After calcination, the morphology and crystallinity of Pd cluster-containing zeolites were still well maintained (Figures S21−S24).

Catalytic activities for H_2 generation from the dehydrogenation of formic acid−sodium formate (FA-SF) (1:1) at 25 and 50 °C are shown in Figures S25 and 3, respectively. Compared to the Pd/C catalyst, Pd cluster-containing zeolite catalysts exhibited complete decomposition of FA as well as superior activities. Moreover, the hydrogen production rates over the Pd/S-1-in catalysts synthesized by in situ encapsulated Pd clusters within nanosized S-1 zeolite are much faster than that over the impregnation-prepared catalyst Pd/S-1-im. Notably, the Pd/S-1-in-K catalyst generated 148 mL of gas without detectable CO (<10 ppm) within 2.0 min (n_{Pd}/n_{FA} = 0.01, FA/SF = 1:1), which is important for fuel cell applications, and the composition of generated gases was confirmed by GC analyses (Figures S26 and S27). Moreover, the Pd/S-1-in-K catalyst gave the highest TOF of 856 h^{-1} at 25 °C and 3027 h^{-1} at 50 °C, which is ~6-fold improvement compared to the Pd/C catalyst. These TOF values are among the highest achieved for heterogeneously catalyzed FA decomposition under similar conditions[3a,c,d,4a] and even higher than those obtained with most of the active homogeneous catalysts (Table S2).[5c,17]

The superior catalytic activities for H_2 generation over Pd/S-1-in-K catalyst could be attributed to the ultrasmall size of the Pd clusters as well as the basicity generated by the introduction of alkali cations onto the zeolites that can act as proton scavengers, favorable for the cleavage of O−H bonds in the FA molecules and subsequent H_2 generation.[7a] The rate of H_2 generation was determined to be 696 L_{H2} h^{-1} g_{Pd}^{-1}, which corresponds to a theoretical power density of 940 W h^{-1} g_{Pd}^{-1} for energy generation.[3c] Assuming 60% operation efficiency and a typical energy requirement value of 0.5−2.0 W h for portable terminals, 0.14−0.56 g of the present Pd/S-1-in-K catalyst would be sufficient to supply H_2 for small proton exchange membrane fuel cell devices.[3d]

Catalytic activities for H_2 generation from the dehydrogenation of FA-SF (1:1) at 50 °C were also investigated over the Pd/S-1-in catalysts with different Pd loading amounts. The catalysts with Pd loadings of 0.47 and 1.08 wt%, with visually observed NP sizes of 1.6 and 2.2 nm (Figure S28), gave TOF values of 2204 and 2119 h^{-1}, respectively, which are comparable with the TOF value of 2197 h^{-1} of the above-studied catalyst with Pd loading content of 0.64 wt% (Figure S29). This result further implies that the intrinsic metal cluster sizes of Pd inside the zeolite channels for catalysts with different Pd loadings are in fact similar.

DOI: 10.1021/jacs.6b03518
J. Am. Chem. Soc. 2016, 138, 7484−7487

To investigate the effect of SF in the dehydrogenation of FA, different ratios of FA and SF were modulated for the Pd/S-1-in-K catalyst. As shown in Figure S30, the activities of FA decomposition improved with increasing molar percentage of SF in the FA-SF solution until the ratio of FA and SF reached 1:1. After that, further increasing the SF percentage had no effect on the FA decomposition. In addition, the reaction temperature also greatly affected the H_2 generation rates. With increasing reaction temperature, the H_2 evolution rates were further enhanced (Figures S31 and S32). The apparent activation energies (E_a) of Pd/S-1-in-K and Pd/S-1-in catalysts were 39.2 and 42.8 kJ mol^{-1}, respectively, which are lower than most of those reported in previous works for FA decomposition (Table S3), indicating that highly efficient H_2 generation from FA can be easily achieved at convenient temperatures.[18]

The recycling stability of FA dehydrogenation over Pd/S-1-in-K and Pd/S-1-in catalysts was investigated. After completion of the previous run, the catalysts were re-collected and dried for the next cycle without reduction again. As shown in Figures S33 and S34, activities were almost the same as that obtained with the fresh catalyst over five cycles. In addition, after the catalytic reaction, the size distributions of Pd clusters as well as the morphology and crystallinity of the zeolite catalysts remained unchanged, suggesting that the catalysts of ultrasmall Pd clusters encapsulated within nanosized S-1 zeolites had superior recycling stabilities during FA decomposition (Figures S35−S39).

In summary, a facile strategy has been successfully developed to synthesize ultrasmall Pd clusters encapsulated within the intersectional channels of nanosized S-1 zeolite using $[Pd(NH_2CH_2CH_2NH_2)_2]Cl_2$ as precursor under direct hydrothermal conditions. The as-prepared catalysts show an excellent activity and highly efficient H_2 generation, without generating CO, toward the complete decomposition of FA in a FA-SF system under mild conditions. Notably, the Pd/S-1-in-K catalyst with incorporated basicity affords the highest TOF values, reaching up to 856 h^{-1} at 25 °C and 3027 h^{-1} at 50 °C, due to the further reduced Pd cluster size and basic sites introduced in the zeolites. In addition, the as-synthesized catalysts possess superior thermal stabilities as well as excellent recycling stabilities during FA decomposition due to the good confinement of Pd clusters within the zeolite matrix. This work demonstrates that zeolites with well-confined nanospaces and shape-selectivity for molecules can be used as the excellent catalytic supports for well-dispersed and ultrasmall metallic clusters. The superior catalytic activities, excellent recyclability, high thermal stability, and easy method to fabricate ultrasmall metal clusters confined in zeolites create a new perspective for the practical application of FA as a viable and effective H_2 storage material for fuel cells.

■ ASSOCIATED CONTENT

Supporting Information

The Supporting Information is available free of charge on the ACS Publications website at DOI: 10.1021/jacs.6b03518.

Experimental details, characterization data, catalytic tests, and calculation methods; Scheme S1, Figures S1−S39, and Tables S1−S3 (PDF)

■ AUTHOR INFORMATION

Corresponding Author

*jihong@jlu.edu.cn

Author Contributions

‡N.W. and Q.S. contributed equally.

Notes

The authors declare no competing financial interest.

■ ACKNOWLEDGMENTS

We thank the State Basic Research Project of China (Grant No. 2014CB931802) and the National Natural Science Foundation of China (Grant No: 21320102001).

■ REFERENCES

(1) (a) Zhu, Q.-L.; Xu, Q. *Energy Environ. Sci.* **2015**, *8*, 478. (b) Schlapbach, L.; Zuttel, A. *Nature* **2001**, *414*, 353. (c) Edwards, P. P.; Kuznetsov, V. L.; David, W. I. F.; Brandon, N. P. *Energy Policy* **2008**, *36*, 4356. (d) Satyapal, S.; Petrovic, J.; Read, C.; Thomas, G.; Ordaz, G. *Catal. Today* **2007**, *120*, 246.

(2) (a) Rosi, N. L.; Eckert, J.; Eddaoudi, M.; Vodak, D. T.; Kim, J.; O'Keeffe, M.; Yaghi, O. M. *Science* **2003**, *300*, 1127. (b) Seayad, A. M.; Antonelli, D. M. *Adv. Mater.* **2004**, *16*, 765. (c) Suh, M. P.; Park, H. J.; Prasad, T. K.; Lim, D. W. *Chem. Rev.* **2012**, *112*, 782. (d) Graetz, J. *Chem. Soc. Rev.* **2009**, *38*, 73.

(3) (a) Jiang, K.; Xu, K.; Zou, S.; Cai, W.-B. *J. Am. Chem. Soc.* **2014**, *136*, 4861. (b) Boddien, A.; Junge, H. *Nat. Nanotechnol.* **2011**, *6*, 265. (c) Wang, Z. L.; Yan, J. M.; Ping, Y.; Wang, H. L.; Zheng, W. T.; Jiang, Q. *Angew. Chem., Int. Ed.* **2013**, *52*, 4406. (d) Zhu, Q.-L.; Tsumori, N.; Xu, Q. *Chem. Sci.* **2014**, *5*, 195. (e) Grasemann, M.; Laurenczy, G. *Energy Environ. Sci.* **2012**, *5*, 8171.

(4) (a) Gu, X.; Lu, Z.-H.; Jiang, H.-L.; Akita, T.; Xu, Q. *J. Am. Chem. Soc.* **2011**, *133*, 11822. (b) Enthaler, S.; von Langermann, J.; Schmidt, T. *Energy Environ. Sci.* **2010**, *3*, 1207.

(5) (a) Fellay, C.; Dyson, P. J.; Laurenczy, G. *Angew. Chem., Int. Ed.* **2008**, *47*, 3966. (b) Johnson, T. C.; Morris, D. J.; Wills, M. *Chem. Soc. Rev.* **2010**, *39*, 81. (c) Fukuzumi, S.; Kobayashi, T.; Suenobu, T. *J. Am. Chem. Soc.* **2010**, *132*, 1496. (d) Boddien, A.; Loges, B.; Gaertner, F.; Torborg, C.; Fumino, K.; Junge, H.; Ludwig, R.; Beller, M. *J. Am. Chem. Soc.* **2010**, *132*, 8924.

(6) Zhu, Q.-L.; Li, J.; Xu, Q. *J. Am. Chem. Soc.* **2013**, *135*, 10210.

(7) (a) Song, F.-Z.; Zhu, Q.-L.; Tsumori, N.; Xu, Q. *ACS Catal.* **2015**, *5*, 5141. (b) Wang, Z.-L.; Wang, H.-L.; Yan, J.-M.; Ping, Y.; O, S.-I.; Li, S.-J.; Jiang, Q. *Chem. Commun.* **2014**, *50*, 2732.

(8) Dai, H.; Xia, B.; Wen, L.; Du, C.; Su, J.; Luo, W.; Cheng, G. *Appl. Catal., B* **2015**, *165*, 57.

(9) (a) Farrusseng, D.; Tuel, A. *New J. Chem.* **2016**, *40*, 3933. (b) Corma, A.; Garcia, H. *Chem. Soc. Rev.* **2008**, *37*, 2096.

(10) (a) Guczi, L.; Kiricsi, I. *Appl. Catal., A* **1999**, *186*, 375. (b) Li, X.; Iglesia, E. *Chem. Commun.* **2008**, 594.

(11) Guzman, J.; Gates, B. C. *Dalton. Trans.* **2003**, 3303.

(12) Gallezot, P. *Post-Synthesis Modification I*; Springer: Berlin, 2002; Vol. 3, pp 257−305.

(13) (a) Choi, M.; Wu, Z.; Iglesia, E. *J. Am. Chem. Soc.* **2010**, *132*, 9129. (b) Goel, S.; Wu, Z. J.; Zones, S. I.; Iglesia, E. *J. Am. Chem. Soc.* **2012**, *134*, 17688. (c) Goel, S.; Zones, S. I.; Iglesia, E. *J. Am. Chem. Soc.* **2014**, *136*, 15280. (d) Wu, Z.; Goel, S.; Choi, M.; Iglesia, E. *J. Catal.* **2014**, *311*, 458.

(14) (a) Kim, J.; Jo, C.; Lee, S.; Ryoo, R. *J. Mater. Chem. A* **2014**, *2*, 11905. (b) Ahn, J. H.; Kolvenbach, R.; Al-Khattaf, S. S.; Jentys, A.; Lercher, J. A. *ACS Catal.* **2013**, *3*, 817.

(15) Keller, T. C.; Desai, K.; Mitchell, S.; Pérez-Ramírez, J. *ACS Catal.* **2015**, *5*, 5388.

(16) Yamada, Y. M. A.; Yuyama, Y.; Sato, T.; Fujikawa, S.; Uozumi, Y. *Angew. Chem.* **2014**, *126*, 131.

(17) Loges, B.; Boddien, A.; Junge, H.; Beller, M. *Angew. Chem., Int. Ed.* **2008**, *47*, 3962.

(18) (a) Bi, Q. Y.; Du, X. L.; Liu, Y. M.; Cao, Y.; He, H. Y.; Fan, K. N. *J. Am. Chem. Soc.* **2012**, *134*, 8926. (b) Ojeda, M.; Iglesia, E. *Angew. Chem., Int. Ed.* **2009**, *48*, 4800. (c) Bulushev, D. A.; Jia, L.; Beloshapkin, S.; Ross, J. R. H. *Chem. Commun.* **2012**, *48*, 4184.

DOI: 10.1021/jacs.6b03518
J. Am. Chem. Soc. 2016, 138, 7484−7487